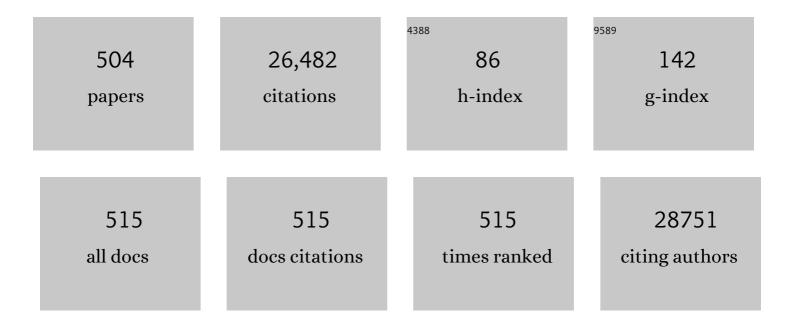
List of Publications by Year in descending order

Source: https://exaly.com/author-pdf/7424878/publications.pdf Version: 2024-02-01



XII IIANRIN

#	Article	IF	CITATIONS
1	High-responsivity graphene/silicon-heterostructure waveguide photodetectors. Nature Photonics, 2013, 7, 888-891.	31.4	731
2	Multifunctional biohybrid magnetite microrobots for imaging-guided therapy. Science Robotics, 2017, 2, .	17.6	594
3	Hybrid Halide Perovskite Solar Cell Precursors: Colloidal Chemistry and Coordination Engineering behind Device Processing for High Efficiency. Journal of the American Chemical Society, 2015, 137, 4460-4468.	13.7	586
4	Graphene and related two-dimensional materials: Structure-property relationships for electronics and optoelectronics. Applied Physics Reviews, 2017, 4, .	11.3	476
5	Iceâ€Templated Assembly Strategy to Construct 3D Boron Nitride Nanosheet Networks in Polymer Composites for Thermal Conductivity Improvement. Small, 2015, 11, 6205-6213.	10.0	473
6	Near-Infrared Photodetector Based on MoS <sub>2</sub> /Black Phosphorus Heterojunction. ACS Photonics, 2016, 3, 692-699.	6.6	446
7	Flexible Piezoelectric-Induced Pressure Sensors for Static Measurements Based on Nanowires/Graphene Heterostructures. ACS Nano, 2017, 11, 4507-4513.	14.6	435
8	Room temperature high-detectivity mid-infrared photodetectors based on black arsenic phosphorus. Science Advances, 2017, 3, e1700589.	10.3	419
9	A Combination of Boron Nitride Nanotubes and Cellulose Nanofibers for the Preparation of a Nanocomposite with High Thermal Conductivity. ACS Nano, 2017, 11, 5167-5178.	14.6	407
10	Polymer Composite with Improved Thermal Conductivity by Constructing a Hierarchically Ordered Three-Dimensional Interconnected Network of BN. ACS Applied Materials & Interfaces, 2017, 9, 13544-13553.	8.0	394
11	Soluble and Stable <i>N</i> â€Heteropentacenes with High Fieldâ€Effect Mobility. Advanced Materials, 2011, 23, 1535-1539.	21.0	334
12	Two-dimensional quasi-freestanding molecular crystals for high-performance organic field-effect transistors. Nature Communications, 2014, 5, 5162.	12.8	315
13	Conducting Polymer Nanostructures: Template Synthesis and Applications in Energy Storage. International Journal of Molecular Sciences, 2010, 11, 2636-2657.	4.1	309
14	The physics and chemistry of graphene-on-surfaces. Chemical Society Reviews, 2017, 46, 4417-4449.	38.1	309
15	Construction of 3D Skeleton for Polymer Composites Achieving a High Thermal Conductivity. Small, 2018, 14, e1704044.	10.0	295
16	Electronic Properties of MoS <sub>2</sub> –WS <sub>2</sub> Heterostructures Synthesized with Two-Step Lateral Epitaxial Strategy. ACS Nano, 2015, 9, 9868-9876.	14.6	283
17	Artificial nacre-like papers based on noncovalent functionalized boron nitride nanosheets with excellent mechanical and thermally conductive properties. Nanoscale, 2015, 7, 6774-6781.	5.6	265
18	Analyzing the Carrier Mobility in Transitionâ€Metal Dichalcogenide MoS <sub>2</sub> Fieldâ€Effect Transistors. Advanced Functional Materials, 2017, 27, 1604093.	14.9	265

#	Article	IF	CITATIONS
19	Highly polarization sensitive infrared photodetector based on black phosphorus-on-WSe 2 photogate vertical heterostructure. Nano Energy, 2017, 37, 53-60.	16.0	252
20	Significant Enhancement of Thermal Conductivity in Bioinspired Freestanding Boron Nitride Papers Filled with Graphene Oxide. Chemistry of Materials, 2016, 28, 1049-1057.	6.7	250
21	Highly Sensitive Glucose Biosensors Based on Organic Electrochemical Transistors Using Platinum Gate Electrodes Modified with Enzyme and Nanomaterials. Advanced Functional Materials, 2011, 21, 2264-2272.	14.9	243
22	Highâ€Performance Grapheneâ€Based Hole Conductorâ€Free Perovskite Solar Cells: Schottky Junction Enhanced Hole Extraction and Electron Blocking. Small, 2015, 11, 2269-2274.	10.0	233
23	Probing Carrier Transport and Structure-Property Relationship of Highly Ordered Organic Semiconductors at the Two-Dimensional Limit. Physical Review Letters, 2016, 116, 016602.	7.8	220
24	A self-powered high-performance graphene/silicon ultraviolet photodetector with ultra-shallow junction: breaking the limit of silicon?. Npj 2D Materials and Applications, 2017, 1, .	7.9	211
25	The Position of Nitrogen in Nâ€Heteropentacenes Matters. Advanced Materials, 2011, 23, 5514-5518.	21.0	210
26	Application of admittance spectroscopy to evaluate carrier mobility in organic charge transport materials. Journal of Applied Physics, 2006, 99, 013706.	2.5	208
27	Through-plane assembly of carbon fibers into 3D skeleton achieving enhanced thermal conductivity of a thermal interface material. Chemical Engineering Journal, 2020, 380, 122550.	12.7	201
28	Polymer composite with enhanced thermal conductivity and mechanical strength through orientation manipulating of BN. Composites Science and Technology, 2018, 160, 127-137.	7.8	199
29	Synergistic Effects of Plasmonics and Electron Trapping in Graphene Short-Wave Infrared Photodetectors with Ultrahigh Responsivity. ACS Nano, 2017, 11, 430-437.	14.6	192
30	1T′ Transition Metal Telluride Atomic Layers for Plasmon-Free SERS at Femtomolar Levels. Journal of the American Chemical Society, 2018, 140, 8696-8704.	13.7	192
31	Lateral Builtâ€In Potential of Monolayer MoS <sub>2</sub> –WS <sub>2</sub> Inâ€Plane Heterostructures by a Shortcut Growth Strategy. Advanced Materials, 2015, 27, 6431-6437.	21.0	191
32	Silver Nanoparticle-Deposited Boron Nitride Nanosheets as Fillers for Polymeric Composites with High Thermal Conductivity. Scientific Reports, 2016, 6, 19394.	3.3	184
33	Recent Advances of Solution-Processed Metal Oxide Thin-Film Transistors. ACS Applied Materials & Interfaces, 2018, 10, 25878-25901.	8.0	183
34	Vertically Aligned and Interconnected SiC Nanowire Networks Leading to Significantly Enhanced Thermal Conductivity of Polymer Composites. ACS Applied Materials & Interfaces, 2018, 10, 9669-9678.	8.0	183
35	Signature of Intrinsic High-Temperature Ferromagnetism in Cobalt-Doped Zinc Oxide Nanocrystals. Advanced Materials, 2006, 18, 2476-2480.	21.0	178
36	Highly Confined and Tunable Hyperbolic Phonon Polaritons in Van Der Waals Semiconducting Transition Metal Oxides. Advanced Materials, 2018, 30, e1705318.	21.0	178

#	Article	IF	CITATIONS
37	2D materials–based homogeneous transistor-memory architecture for neuromorphic hardware. Science, 2021, 373, 1353-1358.	12.6	177
38	Electron Mobility Exceeding 10 cm <sup>2</sup> V <sup>â^'1</sup> s <sup>â î'1</sup> and Bandâ€Like Charge Transport in Solutionâ€Processed nâ€Channel Organic Thinâ€Film Transistors. Advanced Materials, 2016, 28, 5276-5283.	21.0	173
39	The effect of interfacial state on the thermal conductivity of functionalized Al2O3 filled glass fibers reinforced polymer composites. Composites Part A: Applied Science and Manufacturing, 2015, 69, 49-55.	7.6	159
40	Learning from Natural Nacre: Constructing Layered Polymer Composites with High Thermal Conductivity. ACS Applied Materials & amp; Interfaces, 2017, 9, 33001-33010.	8.0	159
41	Evidence of intrinsic ferromagnetism in individual dilute magnetic semiconducting nanostructures. Nature Nanotechnology, 2009, 4, 523-527.	31.5	149
42	Ultrahigh mobility and efficient charge injection in monolayer organic thin-film transistors on boron nitride. Science Advances, 2017, 3, e1701186.	10.3	146
43	Highly Thermally Conductive Composite Papers Prepared Based on the Thought of Bioinspired Engineering. ACS Applied Materials & Interfaces, 2016, 8, 15645-15653.	8.0	145
44	High Responsivity, Broadband, and Fast Graphene/Silicon Photodetector in Photoconductor Mode. Advanced Optical Materials, 2015, 3, 1207-1214.	7.3	141
45	Spray-assisted assembled spherical boron nitride as fillers for polymers with enhanced thermally conductivity. Chemical Engineering Journal, 2019, 370, 166-175.	12.7	141
46	Facile and Environmentally Friendly Solution-Processed Aluminum Oxide Dielectric for Low-Temperature, High-Performance Oxide Thin-Film Transistors. ACS Applied Materials & Interfaces, 2015, 7, 5803-5810.	8.0	139
47	Interfacial Engineering of Silicon Carbide Nanowire/Cellulose Microcrystal Paper toward High Thermal Conductivity. ACS Applied Materials & Interfaces, 2016, 8, 31248-31255.	8.0	139
48	Heat transfer between two metallic surfaces at small distances. Journal of Applied Physics, 1994, 76, 7209-7216.	2.5	134
49	Epitaxial Ultrathin Organic Crystals on Graphene for Highâ€Efficiency Phototransistors. Advanced Materials, 2016, 28, 5200-5205.	21.0	134
50	The role of solution-processed high-κ gate dielectrics in electrical performance of oxide thin-film transistors. Journal of Materials Chemistry C, 2014, 2, 5389.	5.5	133
51	Facile Preparation of Superelastic and Ultralow Dielectric Boron Nitride Nanosheet Aerogels via Freeze-Casting Process. Chemistry of Materials, 2015, 27, 5849-5855.	6.7	133
52	A Paper-Like Inorganic Thermal Interface Material Composed of Hierarchically Structured Graphene/Silicon Carbide Nanorods. ACS Nano, 2019, 13, 1547-1554.	14.6	131
53	Stable and Efficient 3D-2D Perovskite-Perovskite Planar Heterojunction Solar Cell without Organic Hole Transport Layer. Joule, 2018, 2, 2706-2721.	24.0	124
54	Centimeter-Scale CVD Growth of Highly Crystalline Single-Layer MoS <sub>2</sub> Film with Spatial Homogeneity and the Visualization of Grain Boundaries. ACS Applied Materials & Interfaces, 2017, 9, 12073-12081.	8.0	120

#	Article	IF	CITATIONS
55	High-Quality Large-Area Graphene from Dehydrogenated Polycyclic Aromatic Hydrocarbons. Chemistry of Materials, 2012, 24, 3906-3915.	6.7	119
56	Achieving Significant Thermal Conductivity Enhancement via an Ice-Templated and Sintered BN-SiC Skeleton. ACS Applied Materials & Interfaces, 2020, 12, 2892-2902.	8.0	118
57	Graphene controlled Brewster angle device for ultra broadband terahertz modulation. Nature Communications, 2018, 9, 4909.	12.8	117
58	lce-Templated MXene/Ag–Epoxy Nanocomposites as High-Performance Thermal Management Materials. ACS Applied Materials & Interfaces, 2020, 12, 24298-24307.	8.0	117
59	Enhanced thermal conductivity for Ag-deposited alumina sphere/epoxy resin composites through manipulating interfacial thermal resistance. Composites Part A: Applied Science and Manufacturing, 2018, 107, 561-569.	7.6	115
60	Highly Compressive Boron Nitride Nanotube Aerogels Reinforced with Reduced Graphene Oxide. ACS Nano, 2019, 13, 7402-7409.	14.6	115
61	Fusedâ€Ring Electron Acceptor ITICâ€Th: A Novel Stabilizer for Halide Perovskite Precursor Solution. Advanced Energy Materials, 2018, 8, 1703399.	19.5	112
62	Effects of Alkyl Chain Length on Crystal Growth and Oxidation Process of Two-Dimensional Tin Halide Perovskites. ACS Energy Letters, 2020, 5, 1422-1429.	17.4	112
63	Improving thermal conductivity through welding boron nitride nanosheets onto silver nanowires via silver nanoparticles. Composites Science and Technology, 2019, 177, 118-126.	7.8	111
64	Selfâ€Assembled Injectable Nanocomposite Hydrogels Stabilized by Bisphosphonateâ€Magnesium (Mg <sup>2+</sup> ) Coordination Regulates the Differentiation of Encapsulated Stem Cells via Dual Crosslinking. Advanced Functional Materials, 2017, 27, 1701642.	14.9	110
65	Robust Biopolymeric Supramolecular "Hostâ^'Guest Macromer―Hydrogels Reinforced by <i>in Situ</i> Formed Multivalent Nanoclusters for Cartilage Regeneration. Macromolecules, 2016, 49, 866-875.	4.8	102
66	Highly Sensitive and Broadband Organic Photodetectors with Fast Speed Gain and Large Linear Dynamic Range at Low Forward Bias. Small, 2017, 13, 1603260.	10.0	102
67	Highâ€Performance Graphene Devices on SiO <sub>2</sub> /Si Substrate Modified by Highly Ordered Selfâ€Assembled Monolayers. Advanced Materials, 2011, 23, 2464-2468.	21.0	101
68	Boron nitride@graphene oxide hybrids for epoxy composites with enhanced thermal conductivity. RSC Advances, 2016, 6, 35847-35854.	3.6	101
69	A Simple Method for Synthesis of Highâ€Quality Millimeterâ€Scale 1T′ Transitionâ€Metal Telluride and Nearâ€Field Nanooptical Properties. Advanced Materials, 2017, 29, 1700704.	21.0	101
70	Self-assembled N-cadherin mimetic peptide hydrogels promote the chondrogenesis of mesenchymal stem cells through inhibition of canonical Wnt/β-catenin signaling. Biomaterials, 2017, 145, 33-43.	11.4	100
71	Structural evidence of secondary phase segregation from the Raman vibrational modes in Zn1â^'xCoxOâ€^( <x<0.6). .<="" 2007,="" 91,="" applied="" letters,="" physics="" td=""><td>3.3</td><td>98</td></x<0.6).>	3.3	98
72	Band Gap Opening of Bilayer Graphene by F4-TCNQ Molecular Doping and Externally Applied Electric Field. Journal of Physical Chemistry B, 2010, 114, 11377-11381.	2.6	98

#	Article	IF	CITATIONS
73	High-responsivity graphene-on-silicon slot waveguide photodetectors. Nanoscale, 2016, 8, 13206-13211.	5.6	98
74	Improving thermal conductivity of polymer composites by reducing interfacial thermal resistance between boron nitride nanotubes. Composites Science and Technology, 2018, 165, 322-330.	7.8	98
75	Structural, optical and magnetic properties of Co-doped ZnO nanorods with hidden secondary phases. Nanotechnology, 2008, 19, 455702.	2.6	96
76	Ag-Doped Halide Perovskite Nanocrystals for Tunable Band Structure and Efficient Charge Transport. ACS Energy Letters, 2019, 4, 534-541.	17.4	96
77	Graphene Based Nonâ€Volatile Memory Devices. Advanced Materials, 2014, 26, 5496-5503.	21.0	95
78	Selfâ€Assembled Monolayers of Cyclohexylâ€Terminated Phosphonic Acids as a General Dielectric Surface for Highâ€Performance Organic Thinâ€Film Transistors. Advanced Materials, 2014, 26, 7190-7196.	21.0	95
79	Quantitative Analysis of Graphene Doping by Organic Molecular Charge Transfer. Journal of Physical Chemistry C, 2011, 115, 7596-7602.	3.1	94
80	Nonstoichiometric acid–base reaction as reliable synthetic route to highly stable CH3NH3PbI3 perovskite film. Nature Communications, 2016, 7, 13503.	12.8	94
81	Nacre-inspired polymer composites with high thermal conductivity and enhanced mechanical strength. Composites Part A: Applied Science and Manufacturing, 2019, 121, 92-99.	7.6	94
82	Preparation of Boron Nitride Nanosheet/Nanofibrillated Cellulose Nanocomposites with Ultrahigh Thermal Conductivity via Engineering Interfacial Thermal Resistance. Advanced Materials Interfaces, 2017, 4, 1700563.	3.7	93
83	Precise, Self-Limited Epitaxy of Ultrathin Organic Semiconductors and Heterojunctions Tailored by van der Waals Interactions. Nano Letters, 2016, 16, 3754-3759.	9.1	92
84	Spherical core-shell Al@Al2O3 filled epoxy resin composites as high-performance thermal interface materials. Composites Part A: Applied Science and Manufacturing, 2019, 123, 260-269.	7.6	91
85	Raman spectroscopic study of oxidation and phase transition in W18O49 nanowires. Journal of Raman Spectroscopy, 2007, 38, 176-180.	2.5	89
86	Selfâ€Assembled Monolayers of Phosphonic Acids with Enhanced Surface Energy for Highâ€Performance Solutionâ€Processed Nâ€Channel Organic Thinâ€Film Transistors. Angewandte Chemie - International Edition, 2013, 52, 6222-6227.	13.8	89
87	High-Performance Broadband Floating-Base Bipolar Phototransistor Based on WSe <sub>2</sub> /BP/MoS <sub>2</sub> Heterostructure. ACS Photonics, 2017, 4, 823-829.	6.6	89
88	Flexible dielectric papers based on biodegradable cellulose nanofibers and carbon nanotubes for dielectric energy storage. Journal of Materials Chemistry C, 2016, 4, 6037-6044.	5.5	88
89	Graphene size-dependent modulation of graphene frameworks contributing to the superior thermal conductivity of epoxy composites. Journal of Materials Chemistry A, 2018, 6, 12091-12097.	10.3	88
90	Stable and scalable 3D-2D planar heterojunction perovskite solar cells via vapor deposition. Nano Energy, 2019, 59, 619-625.	16.0	88

#	Article	IF	CITATIONS
91	Preparation and characterization of alginate–carrageenan hydrogel films crosslinked using a water-soluble carbodiimide (WSC). Journal of Membrane Science, 2003, 218, 131-146.	8.2	87
92	Molybdenum disulfide-based amplified fluorescence DNA detection using hybridization chain reactions. Journal of Materials Chemistry B, 2015, 3, 2395-2401.	5.8	87
93	NiO mesoporous nanowalls grown on RGO coated nickel foam as high performance electrodes for supercapacitors and biosensors. Electrochimica Acta, 2016, 192, 205-215.	5.2	87
94	Emission enhancement from metallodielectric-capped ZnO films. Journal of Applied Physics, 2006, 100, 026103.	2.5	86
95	Monolayer Fieldâ€Effect Transistors of Nonplanar Organic Semiconductors with Brickwork Arrangement. Advanced Materials, 2015, 27, 3418-3423.	21.0	85
96	Aggregation-based growth and magnetic properties of inhomogeneous Cu-doped ZnO nanocrystals. Applied Physics Letters, 2007, 90, 212502.	3.3	82
97	General Nondestructive Passivation by 4â€Fluoroaniline for Perovskite Solar Cells with Improved Performance and Stability. Small, 2018, 14, e1803350.	10.0	82
98	Hollow SnO2@Co3O4 core–shell spheres encapsulated in three-dimensional graphene foams for high performance supercapacitors and lithium-ion batteries. Journal of Power Sources, 2015, 298, 83-91.	7.8	80
99	Near-infrared light-triggered release of small molecules for controlled differentiation and long-term tracking of stem cells inÂvivo using upconversion nanoparticles. Biomaterials, 2016, 110, 1-10.	11.4	77
100	Hybrid graphene tunneling photoconductor with interface engineering towards fast photoresponse and high responsivity. Npj 2D Materials and Applications, 2017, 1, .	7.9	77
101	Short Range Order and the Nature of Defects and Traps in Amorphous Silicon Oxynitride Governed by the Mott Rule. Physical Review Letters, 1998, 81, 1054-1057.	7.8	76
102	N-heteroquinones: quadruple weak hydrogen bonds and n-channel transistors. Chemical Communications, 2010, 46, 2977.	4.1	76
103	ZnO-nanorods/graphene heterostructure: a direct electron transfer glucose biosensor. Scientific Reports, 2016, 6, 32327.	3.3	76
104	Flexible graphene electrothermal films made from electrochemically exfoliated graphite. Journal of Materials Science, 2016, 51, 1043-1051.	3.7	76
105	Largeâ€Grain Formamidinium PbI <sub>3–</sub> <i><sub>x</sub></i> Br <i><sub>x</sub></i> for Highâ€Performance Perovskite Solar Cells via Intermediate Halide Exchange. Advanced Energy Materials, 2017, 7, 1601882.	19.5	76
106	In-Plane Optical Absorption and Free Carrier Absorption in Graphene-on-Silicon Waveguides. IEEE Journal of Selected Topics in Quantum Electronics, 2014, 20, 43-48.	2.9	75
107	Textured CH3NH3PbI3 thin film with enhanced stability for high performance perovskite solar cells. Nano Energy, 2017, 33, 485-496.	16.0	74
108	Crystallinity Preservation and Ion Migration Suppression through Dual Ion Exchange Strategy for Stable Mixed Perovskite Solar Cells. Advanced Energy Materials, 2017, 7, 1700118.	19.5	74

#	Article	IF	CITATIONS
109	Epitaxial Stitching and Stacking Growth of Atomically Thin Transitionâ€Metal Dichalcogenides (TMDCs) Heterojunctions. Advanced Functional Materials, 2017, 27, 1603884.	14.9	73
110	Ultrathin efficient perovskite solar cells employing a periodic structure of a composite hole conductor for elevated plasmonic light harvesting and hole collection. Nanoscale, 2016, 8, 6290-6299.	5.6	69
111	Fully Biodegradable Water Droplet Energy Harvester Based on Leaves of Living Plants. ACS Applied Materials & Interfaces, 2020, 12, 56060-56067.	8.0	69
112	Oxygen gettering and oxide degradation during annealing of Si/SiO2/Si structures. Journal of Applied Physics, 1995, 77, 175-186.	2.5	68
113	Performance and Stability Improvement of P3HT:PCBM-Based Solar Cells by Thermally Evaporated Chromium Oxide (CrO <sub><i>x</i></sub> ) Interfacial Layer. ACS Applied Materials & Interfaces, 2010, 2, 2699-2702.	8.0	68
114	Short-range order in non-stoichiometric amorphous silicon oxynitride and silicon-rich nitride. Journal of Non-Crystalline Solids, 2002, 297, 96-101.	3.1	67
115	Induced Crystallization of Rubrene in Thinâ€Film Transistors. Advanced Materials, 2010, 22, 3242-3246.	21.0	67
116	A novel fluorescence "on-off-on―peptide-based chemosensor for simultaneous detection of Cu2+, Ag+ and S2â''. Sensors and Actuators B: Chemical, 2019, 280, 129-137.	7.8	67
117	Duallyâ€Passivated Perovskite Solar Cells with Reduced Voltage Loss and Increased Super Oxide Resistance. Angewandte Chemie, 2021, 133, 8384-8393.	2.0	66
118	Structure control and characterization of SrBi2Ta2O9 thin films by a modified annealing method. Applied Physics Letters, 1999, 74, 1221-1223.	3.3	65
119	Degradation mechanism of organic solar cells with aluminum cathode. Solar Energy Materials and Solar Cells, 2011, 95, 3303-3310.	6.2	65
120	Restoring the photovoltaic effect in graphene-based van der Waals heterojunctions towards self-powered high-detectivity photodetectors. Nano Energy, 2019, 57, 214-221.	16.0	65
121	Interlayer Interaction Enhancement in Ruddlesden–Popper Perovskite Solar Cells toward High Efficiency and Phase Stability. ACS Energy Letters, 2019, 4, 1025-1033.	17.4	64
122	Three-dimensional interconnected graphene microsphere as fillers for enhancing thermal conductivity of polymer. Chemical Engineering Journal, 2019, 368, 79-87.	12.7	64
123	A Meaningful Analogue of Pentacene: Charge Transport, Polymorphs, and Electronic Structures of Dihydrodiazapentacene. Chemistry of Materials, 2009, 21, 1400-1405.	6.7	63
124	Fibrous Epoxy Substrate with High Thermal Conductivity and Low Dielectric Property for Flexible Electronics. Advanced Electronic Materials, 2016, 2, 1500485.	5.1	63
125	Perovskite Bifunctional Device with Improved Electroluminescent and Photovoltaic Performance through Interfacial Energyâ€Band Engineering. Advanced Materials, 2019, 31, e1902543.	21.0	62
126	Low-Voltage Organic Field-Effect Transistors (OFETs) with Solution-Processed Metal-Oxide as Gate Dielectric. ACS Applied Materials & Interfaces, 2011, 3, 4662-4667.	8.0	61

#	Article	IF	CITATIONS
127	Aqueous Solution-Deposited Gallium Oxide Dielectric for Low-Temperature, Low-Operating-Voltage Indium Oxide Thin-Film Transistors: A Facile Route to Green Oxide Electronics. ACS Applied Materials & Interfaces, 2015, 7, 14720-14725.	8.0	60
128	Conformational manipulation of scale-up prepared single-chain polymeric nanogels for multiscale regulation of cells. Nature Communications, 2019, 10, 2705.	12.8	60
129	Strong optical response and light emission from a monolayer molecular crystal. Nature Communications, 2019, 10, 5589.	12.8	59
130	Enhancing lightâ€matter interaction in <scp>2D</scp> materials by optical micro/nano architectures for highâ€performance optoelectronic devices. InformaÄnÃ-MateriA¡ly, 2021, 3, 36-60.	17.3	59
131	Enhanced optical Kerr nonlinearity of MoS_2 on silicon waveguides. Photonics Research, 2015, 3, 206.	7.0	58
132	Observation of a giant two-dimensional band-piezoelectric effect on biaxial-strained graphene. NPG Asia Materials, 2015, 7, e154-e154.	7.9	58
133	Highly thermally conductive polymer nanocomposites based on boron nitride nanosheets decorated with silver nanoparticles. RSC Advances, 2016, 6, 41630-41636.	3.6	58
134	Silver Telluride Nanowire Assembly for Highâ€Performance Flexible Thermoelectric Film and Its Application in Selfâ€Powered Temperature Sensor. Advanced Electronic Materials, 2019, 5, 1800612.	5.1	58
135	In situobservation of the ferroelectric-paraelectric phase transition in a triglycine sulfate single crystal by variable-temperature electrostatic force microscopy. Physical Review B, 2000, 61, 203-206.	3.2	57
136	Core–shell Cu@rGO hybrids filled in epoxy composites with high thermal conduction. Journal of Materials Chemistry C, 2018, 6, 257-265.	5.5	56
137	Terahertz Microfluidic Metamaterial Biosensor for Sensitive Detection of Small-Volume Liquid Samples. IEEE Transactions on Terahertz Science and Technology, 2019, 9, 209-214.	3.1	56
138	Guanidinium doping enabled low-temperature fabrication of high-efficiency all-inorganic CsPbI <sub>2</sub> Br perovskite solar cells. Journal of Materials Chemistry A, 2019, 7, 27640-27647.	10.3	56
139	Integration of inverse nanocone array based bismuth vanadate photoanodes and bandgap-tunable perovskite solar cells for efficient self-powered solar water splitting. Journal of Materials Chemistry A, 2017, 5, 19091-19097.	10.3	55
140	Abnormal Synergetic Effect of Organic and Halide Ions on the Stability and Optoelectronic Properties of a Mixed Perovskite via In Situ Characterizations. Advanced Materials, 2018, 30, e1801562.	21.0	55
141	Recent progress in thermally conductive polymer/boron nitride composites by constructing three-dimensional networks. Composites Communications, 2021, 24, 100650.	6.3	55
142	Radial ZnO nanowire nucleation on amorphous carbons. Applied Physics Letters, 2005, 87, 183109.	3.3	53
143	Molecular cargo delivery using multicellular magnetic microswimmers. Applied Materials Today, 2019, 15, 242-251.	4.3	52
144	Identifying the functional groups effect on passivating perovskite solar cells. Science Bulletin, 2020, 65, 1726-1734.	9.0	52

#	Article	IF	CITATIONS
145	Solution-Processed Ambipolar Organic Thin-Film Transistors by Blending p- and n-Type Semiconductors: Solid Solution versus Microphase Separation. ACS Applied Materials & Interfaces, 2015, 7, 28019-28026.	8.0	51
146	High hole mobility of 1,2-bis[4′-(diphenylamino)biphenyl-4-yl]-1,2-diphenylethene in field effect transistor. Chemical Communications, 2011, 47, 6924.	4.1	50
147	Mechanical reinforcement while remaining electrical insulation of glass fibre/polymer composites using core–shell CNT@SiO 2 hybrids as fillers. Composites Part A: Applied Science and Manufacturing, 2015, 73, 260-268.	7.6	50
148	Multifunctional Quantum Dot Nanoparticles for Effective Differentiation and Longâ€Term Tracking of Human Mesenchymal Stem Cells In Vitro and In Vivo. Advanced Healthcare Materials, 2016, 5, 1049-1057.	7.6	50
149	Growth of Large-Scale, Large-Size, Few-Layered α-MoO <sub>3</sub> on SiO <sub>2</sub> and Its Photoresponse Mechanism. ACS Applied Materials & Interfaces, 2017, 9, 5543-5549.	8.0	50
150	A novel h-BN–RGO hybrids for epoxy resin composites achieving enhanced high thermal conductivity and energy density. RSC Advances, 2017, 7, 23355-23362.	3.6	50
151	Imperfect oriented attachment: Direct activation of high-temperature ferromagnetism in diluted magnetic semiconductor nanocrystals. Applied Physics Letters, 2006, 88, 223108.	3.3	49
152	Controlling of the surface energy of the gate dielectric in organic field-effect transistors by polymer blend. Applied Physics Letters, 2009, 94, .	3.3	48
153	Single crystal n-channel field effect transistors from solution-processed silylethynylated tetraazapentacene. Journal of Materials Chemistry, 2011, 21, 15201.	6.7	48
154	Fully solution-processed metal oxide thin-film transistors via a low-temperature aqueous route. Ceramics International, 2017, 43, 6130-6137.	4.8	48
155	Carbon Dot-Based Composite Films for Simultaneously Harvesting Raindrop Energy and Boosting Solar Energy Conversion Efficiency in Hybrid Cells. ACS Nano, 2020, 14, 10359-10369.	14.6	47
156	Synthesis and Characterization of Metallic Janus MoSH Monolayer. ACS Nano, 2021, 15, 20319-20331.	14.6	47
157	Graphene photodetector integrated on silicon nitride waveguide. Journal of Applied Physics, 2015, 117, .	2.5	46
158	Controlled Electrochemical Deposition of Largeâ€Area MoS <sub>2</sub> on Graphene for Highâ€Responsivity Photodetectors. Advanced Functional Materials, 2017, 27, 1603998.	14.9	45
159	Silver nanoparticle-modified alumina microsphere hybrid composites for enhanced energy density and thermal conductivity. Composites Part A: Applied Science and Manufacturing, 2019, 119, 299-309.	7.6	45
160	Artificial control of in-plane anisotropic photoelectricity in monolayer MoS2. Applied Materials Today, 2019, 15, 203-211.	4.3	45
161	Low-temperature preparation and characterization of SrBi2Ta2O9 thin films on (100)-oriented LaNiO3 electrodes. Applied Physics Letters, 2000, 76, 1758-1760.	3.3	44
162	Low-temperature facile solution-processed gate dielectric for combustion derived oxide thin film transistors. RSC Advances, 2014, 4, 54729-54739.	3.6	44

#	Article	IF	CITATIONS
163	Manipulating Orientation of Silicon Carbide Nanowire in Polymer Composites to Achieve High Thermal Conductivity. Advanced Materials Interfaces, 2017, 4, 1700446.	3.7	43
164	Boron nitride microsphere/epoxy composites with enhanced thermal conductivity. High Voltage, 2017, 2, 147-153.	4.7	43
165	An Interlayer with Strong Pb-Cl Bond Delivers Ultraviolet-Filter-Free, Efficient, and Photostable Perovskite Solar Cells. IScience, 2019, 21, 217-227.	4.1	43
166	Hybrid 2Dâ€Material Photonics with Bound States in the Continuum. Advanced Optical Materials, 2019, 7, 1901306.	7.3	43
167	Thickness dependence of mobility in CuPc thin film on amorphous SiO2 substrate. Journal Physics D: Applied Physics, 2007, 40, 5666-5669.	2.8	42
168	Nanocarrierâ€Mediated Codelivery of Small Molecular Drugs and siRNA to Enhance Chondrogenic Differentiation and Suppress Hypertrophy of Human Mesenchymal Stem Cells. Advanced Functional Materials, 2016, 26, 2463-2472.	14.9	42
169	Study of domain stability on (Pb0.76Ca0.24)TiO3 thin films using piezoresponse microscopy. Applied Physics Letters, 2002, 81, 715-717.	3.3	41
170	GaAsSb/GaAs band alignment evaluation for long-wave photonic applications. Journal of Crystal Growth, 2003, 251, 521-525.	1.5	41
171	Scaling Dopant States in a Semiconducting Nanostructure by Chemically Resolved Electron Energy-Loss Spectroscopy: A Case Study on Co-Doped ZnO. Journal of the American Chemical Society, 2010, 132, 6492-6497.	13.7	41
172	Device lifetime improvement of polymer-based bulk heterojunction solar cells by incorporating copper oxide layer at Al cathode. Applied Physics Letters, 2011, 98, .	3.3	41
173	The influence of gate dielectrics on a high-mobility n-type conjugated polymer in organic thin-film transistors. Applied Physics Letters, 2012, 100, 033301.	3.3	41
174	Graphene Based Terahertz Light Modulator in Total Internal Reflection Geometry. Advanced Optical Materials, 2017, 5, 1600697.	7.3	41
175	Ultraâ€Low Work Function Transparent Electrodes Achieved by Naturally Occurring Biomaterials for Organic Optoelectronic Devices. Advanced Materials Interfaces, 2014, 1, 1400215.	3.7	40
176	Encapsulating carbon nanotubes with SiO <sub>2</sub> : a strategy for applying them in polymer nanocomposites with high mechanical strength and electrical insulation. Journal of Materials Chemistry C, 2015, 3, 187-195.	5.5	40
177	Transistors from a conjugated macrocycle molecule: field and photo effects. Chemical Communications, 2008, , 4324.	4.1	39
178	Nanoantenna‣andwiched Graphene with Giant Spectral Tuning in the Visibleâ€ŧoâ€Nearâ€Infrared Region. Advanced Optical Materials, 2014, 2, 162-170.	7.3	39
179	Asymmetric Alkynylative Ring Opening Reaction of Oxabenzonorbornadienes Promoted by Palladium/Silver Cocatalytic System. Advanced Synthesis and Catalysis, 2014, 356, 2960-2964.	4.3	39
180	Thicknessâ€Dependent Optical Properties and Inâ€Plane Anisotropic Raman Response of the 2D βâ€In 2 S 3. Advanced Optical Materials, 2019, 7, 1901085.	7.3	39

#	Article	IF	CITATIONS
181	Interlayer Cross‣inked 2D Perovskite Solar Cell with Uniform Phase Distribution and Increased Exciton Coupling. Solar Rrl, 2020, 4, 1900578.	5.8	39
182	Understanding Charge Transport in All-Inorganic Halide Perovskite Nanocrystal Thin-Film Field Effect Transistors. ACS Energy Letters, 2020, 5, 2614-2623.	17.4	39
183	Palladium/Copper Complexes Coâ€Catalyzed Highly Enantioselective Ring Opening Reaction of Azabenzonorbornadienes with Terminal Alkynes. Advanced Synthesis and Catalysis, 2013, 355, 2827-2832.	4.3	38
184	High-Quality Monolithic Graphene Films via Laterally Stitched Growth and Structural Repair of Isolated Flakes for Transparent Electronics. Chemistry of Materials, 2017, 29, 7808-7815.	6.7	38
185	Functionalized ï€ Stacks of Hexabenzoperylenes as a Platform for Chemical and Biological Sensing. CheM, 2018, 4, 1416-1426.	11.7	38
186	Magnetic domain structures of Co22Ag78 granular films observed by magnetic force microscopy. Applied Physics Letters, 1998, 72, 2472-2474.	3.3	36
187	Al incorporation, structural and optical properties of AlxGa1â^'xN (0.13⩽x⩽0.8) alloys grown by MOCVD. Journal of Crystal Growth, 2008, 310, 4499-4502.	1.5	36
188	Self-Assembly of PTCDA Ultrathin Films on Graphene: Structural Phase Transition and Charge Transfer Saturation. Journal of Physical Chemistry C, 2010, 114, 20917-20924.	3.1	36
189	A highly thermally conductive electrode for lithium ion batteries. Journal of Materials Chemistry A, 2016, 4, 14595-14604.	10.3	36
190	Graphene/In <sub>2</sub> S <sub>3</sub> van der Waals Heterostructure for Ultrasensitive Photodetection. ACS Photonics, 2018, 5, 4912-4919.	6.6	36
191	van der Waals Transition-Metal Oxide for Vis–MIR Broadband Photodetection via Intercalation Strategy. ACS Applied Materials & Interfaces, 2019, 11, 15741-15747.	8.0	36
192	In Situ Ultrafast and Patterned Growth of Transition Metal Dichalcogenides from Inkjetâ€Printed Aqueous Precursors. Advanced Materials, 2021, 33, e2100260.	21.0	36
193	Room-Temperature Welding of Silver Telluride Nanowires for High-Performance Thermoelectric Film. ACS Applied Materials & Interfaces, 2019, 11, 37892-37900.	8.0	35
194	Energy-exchange processes by tunneling electrons. Applied Physics A: Solids and Surfaces, 1994, 59, 155-161.	1.4	34
195	Angle resolved surface enhanced Raman scattering (SERS) on two-dimensional metallic arrays with different hole sizes. Applied Physics Letters, 2010, 96, 033104.	3.3	34
196	Solution-processed PCDTBT capped low-voltage InGaZnOx thin film phototransistors for visible-light detection. Applied Physics Letters, 2015, 106, .	3.3	34
197	Efficient ternary bulk heterojunction solar cells with PCDTBT as hole-cascade material. Nano Energy, 2016, 19, 476-485.	16.0	34
198	High-speed infrared two-dimensional platinum diselenide photodetectors. Applied Physics Letters, 2020, 116, .	3.3	33

#	Article	IF	CITATIONS
199	Nanoparticles with rationally designed isoelectronic traps as fillers significantly enhance breakdown strength and electrostatic energy density of polymer composites. Composites Science and Technology, 2020, 195, 108201.	7.8	33
200	Efficient Slantwise Aligned Dion–Jacobson Phase Perovskite Solar Cells Based on Transâ€1,4â€Cyclohexanediamine. Small, 2020, 16, e2003098.	10.0	33
201	Domain imaging and local piezoelectric properties of the (200)-predominant SrBi2Ta2O9 thin film. Applied Physics Letters, 1999, 75, 1610-1612.	3.3	32
202	Dependence of surface plasmon lifetimes on the hole size in two-dimensional metallic arrays. Applied Physics Letters, 2009, 94, 183112.	3.3	32
203	Graphene/Metal Contacts: Bistable States and Novel Memory Devices. Advanced Materials, 2012, 24, 2614-2619.	21.0	32
204	Facile passivation of solution-processed InZnO thin-film transistors by octadecylphosphonic acid self-assembled monolayers at room temperature. Applied Physics Letters, 2014, 104, .	3.3	32
205	Rhodium( <scp>i</scp> )-catalysed decarbonylative direct C–H vinylation and dienylation of arenes. Organic Chemistry Frontiers, 2018, 5, 734-740.	4.5	32
206	Bound-States-in-Continuum Hybrid Integration of 2D Platinum Diselenide on Silicon Nitride for High-Speed Photodetectors. ACS Photonics, 2020, 7, 2643-2649.	6.6	32
207	Plasmonic optical trap having very large active volume realized with nano-ring structure. Optics Letters, 2012, 37, 1748.	3.3	31
208	Control of interfacial silicate between HfO2 and Si by high concentration ozone. Applied Physics Letters, 2006, 88, 072903.	3.3	30
209	Enhanced Reduction of Graphene Oxide on Recyclable Cu Foils to Fabricate Graphene Films with Superior Thermal Conductivity. Scientific Reports, 2015, 5, 14260.	3.3	30
210	Effects of 3d transition-metal doping on electronic and magnetic properties of MoS2nanoribbons. Physical Chemistry Chemical Physics, 2015, 17, 1831-1836.	2.8	30
211	Realization of vertical and lateral van der Waals heterojunctions using two-dimensional layered organic semiconductors. Nano Research, 2017, 10, 1336-1344.	10.4	30
212	Surface Polarity Regulation by Relieving Fermi‣evel Pinning with Naphthalocyanine Tetraimides toward Efficient Perovskite Solar Cells with Improved Photostability. Advanced Energy Materials, 2022, 12, .	19.5	30
213	Spectroscopic Study of Electron and Hole Polarons in a High-Mobility Donor–Acceptor Conjugated Copolymer. Journal of Physical Chemistry C, 2013, 117, 6835-6841.	3.1	29
214	Interface Engineering for CVD Graphene: Current Status and Progress. Small, 2014, 10, 4443-4454.	10.0	29
215	Real-time visualization of thermally activated degradation of the ITO/CuPC/NPB/Alq3stack used in one of the organic light-emitting diodes. Journal Physics D: Applied Physics, 2004, 37, 1603-1608.	2.8	28
216	Electronic Properties of Graphene Altered by Substrate Surface Chemistry and Externally Applied Electric Field. Journal of Physical Chemistry C, 2012, 116, 6259-6267.	3.1	28

#	Article	IF	CITATIONS
217	Controllable modulation of the electronic properties of graphene and silicene by interface engineering and pressure. Journal of Materials Chemistry C, 2013, 1, 4869.	5.5	28
218	Metal dopants in HfO <sub>2</sub> -based RRAM: first principle study. Journal of Semiconductors, 2014, 35, 042002.	3.7	28
219	Ternary Bulk Heterojunction Photovoltaic Cells Composed of Small Molecule Donor Additive as Cascade Material. Journal of Physical Chemistry C, 2014, 118, 20094-20099.	3.1	28
220	Bioactive Nanocomposite Poly (Ethylene Glycol) Hydrogels Crosslinked by Multifunctional Layered Double Hydroxides Nanocrosslinkers. Macromolecular Bioscience, 2016, 16, 1019-1026.	4.1	28
221	Uncovering the Electronâ€Phonon Interplay and Dynamical Energyâ€Dissipation Mechanisms of Hot Carriers in Hybrid Lead Halide Perovskites. Advanced Energy Materials, 2021, 11, 2003071.	19.5	28
222	Electron field emission from SiC/Si heterostructures synthesized by carbon implantation using a metal vapor vacuum arc ion source. Applied Physics Letters, 1998, 72, 1926-1928.	3.3	27
223	Room temperature visible electroluminescence in silicon nanostructures. Journal of Vacuum Science and Technology A: Vacuum, Surfaces and Films, 1999, 17, 159-163.	2.1	27
224	Bonding and band offset in N[sub 2]O-grown oxynitride. Journal of Vacuum Science & Technology an Official Journal of the American Vacuum Society B, Microelectronics Processing and Phenomena, 2003, 21, 241.	1.6	27
225	Quantitative determination of scattering mechanism in large-area graphene on conventional and SAM-functionalized substrates at room temperature. Nanoscale, 2013, 5, 5784.	5.6	27
226	Enhanced Performance and Fermi-Level Estimation of Coronene-Derived Graphene Transistors on Self-Assembled Monolayer Modified Substrates in Large Areas. Journal of Physical Chemistry C, 2013, 117, 4800-4807.	3.1	27
227	Efficient Electronic Transport in Partially Disordered Co <sub>3</sub> O <sub>4</sub> Nanosheets for Electrocatalytic Oxygen Evolution Reaction. ACS Applied Energy Materials, 2020, 3, 3071-3081.	5.1	27
228	Probing the conducting paths in a metal - insulator composite by conducting atomic force microscopy. Journal Physics D: Applied Physics, 1996, 29, 3169-3172.	2.8	26
229	Structural enhancement mechanism of field emission from multilayer semiconductor films. Physical Review B, 2005, 72, .	3.2	26
230	Controllable Modulation of the Electronic Structure of ZnO(101Ì0) Surface by Carboxylic Acids. Journal of Physical Chemistry C, 2010, 114, 3973-3980.	3.1	26
231	Deterministic and Etchingâ€Free Transfer of Largeâ€Scale 2D Layered Materials for Constructing Interlayer Coupled van der Waals Heterostructures. Advanced Materials Technologies, 2018, 3, 1700282.	5.8	26
232	An Acoustic Metaâ€ <del>S</del> kin Insulator. Advanced Materials, 2020, 32, e2002251.	21.0	26
233	Quantitative Analysis of Scattering Mechanisms in Highly Crystalline CVD MoS <sub>2</sub> through a Self-Limited Growth Strategy by Interface Engineering. Small, 2016, 12, 438-445.	10.0	25
234	Thermal sensors for investigation of heat transfer in scanning probe microscopy. Review of Scientific Instruments, 1994, 65, 2262-2266.	1.3	24

#	Article	IF	CITATIONS
235	Study of Excess Silicon at Si3 N 4 / Thermal SiO2 Interface Using EELS and Ellipsometric Measu Journal of the Electrochemical Society, 1999, 146, 780-785.	rements. 2.9	24
236	Alginic acid–silica hydrogel coatings for the protection of osmotic distillation membranes against wet-out by surface-active agents. Journal of Membrane Science, 2005, 260, 19-25.	8.2	24
237	Improving lateral resolution of electrostatic force microscopy by multifrequency method under ambient conditions. Applied Physics Letters, 2009, 94, 223109.	3.3	24
238	3D RGO frameworks wrapped hollow spherical SnO 2 -Fe 2 O 3 mesoporous nano-shells: fabrication, characterization and lithium storage properties. Electrochimica Acta, 2016, 202, 186-196.	5.2	24
239	Broadside Nanoantennas Made of Single Silver Nanorods. ACS Nano, 2018, 12, 1720-1731.	14.6	24
240	Green perovskite light-emitting diodes with simultaneous high luminance and quantum efficiency through charge injection engineering. Science Bulletin, 2020, 65, 1832-1839.	9.0	24
241	Surface Morphology of Ferroelectric Domains inBaTiO3Single Crystals: An Atomic Force Microscope Study. Japanese Journal of Applied Physics, 1997, 36, 5566-5569.	1.5	23
242	Optical and electrical properties of nitrogen incorporated amorphous carbon films. Journal of Applied Physics, 2000, 87, 2874-2879.	2.5	23
243	Nanoscale <i>in situ</i> investigation of ultrathin silicon oxide thermal decomposition by high temperature scanning tunneling microscopy. Nanotechnology, 2007, 18, 485709.	2.6	23
244	Enhanced Performance of Polymeric Bulk Heterojunction Solar Cells via Molecular Doping with TFSA. ACS Applied Materials & Interfaces, 2015, 7, 13415-13421.	8.0	23
245	Nearâ€Infrared Photoresponse of Oneâ€Sided Abrupt MAPbI <sub>3</sub> /TiO <sub>2</sub> Heterojunction through a Tunneling Process. Advanced Functional Materials, 2016, 26, 8545-8554.	14.9	23
246	Self-driven hematite-based photoelectrochemical water splitting cells with three-dimensional nanobowl heterojunction and high-photovoltage perovskite solar cells. Materials Today Energy, 2017, 6, 128-135.	4.7	23
247	Polymer composites with high thermal conductivity optimized by polyline-folded graphite paper. Composites Science and Technology, 2020, 188, 107970.	7.8	23
248	ZnO electron transporting layer engineering realized over 20% efficiency and over 1.28 V openâ€circuit voltage in allâ€inorganic perovskite solar cells. EcoMat, 2022, 4, .	11.9	23
249	Oxygen plasma assisted high performance solution-processed Al2Ox gate insulator for combustion-processed InGaZnOx thin film transistors. Journal of Applied Physics, 2015, 117, .	2.5	22
250	Effects of a Bi4Ti3O12 buffer layer on SrBi2Ta2O9 thin films prepared by the metalorganic decomposition. Applied Physics Letters, 1999, 74, 3711-3713.	3.3	21
251	Study of microscopic piezoelectricity of (Pb0.76Ca0.24)TiO3 thin films. Physics Letters, Section A: General, Atomic and Solid State Physics, 2002, 294, 217-221.	2.1	21
252	Nanoscale investigation of moisture-induced degradation mechanisms of tris(8-hydroxyquinoline) aluminium-based organic light-emitting diodes. Journal Physics D: Applied Physics, 2004, 37, 2618-2622.	2.8	21

#	Article	IF	CITATIONS
253	Effects of plasma immersion ion nitridation on dielectric properties of HfO2. Applied Physics Letters, 2007, 90, 122901.	3.3	21
254	Insights into the Interfacial Properties of Low-Voltage CuPc Field-Effect Transistor. ACS Applied Materials & Interfaces, 2013, 5, 4960-4965.	8.0	21
255	Enhanced four-wave mixing with MoS <sub>2</sub> on a silicon waveguide. Journal of Optics (United) Tj ETQq1	1 0.78431 2.2	4 rgBT /Ove
256	Enhanced Electrochemical Stability by Alkyldiammonium in Dion–Jacobson Perovskite toward Ultrastable Lightâ€Emitting Diodes. Advanced Optical Materials, 2021, 9, 2100243.	7.3	21
257	Surface morphology of metalorganic vapor phase epitaxy grown strainedâ€layer InxGa1â^'xAs on GaAs observed by atomic force microscopy. Applied Physics Letters, 1995, 66, 604-606.	3.3	20
258	Electrical properties of nitrogen incorporated tetrahedral amorphous carbon films. Thin Solid Films, 1999, 339, 74-77.	1.8	20
259	Vacuum electron emission with low turn-on electric field from hydrogenated amorphous carbon thin films. Applied Physics Letters, 2001, 79, 141-143.	3.3	20
260	Homo- and Hetero- p–n Junctions Formed on Graphene Steps. ACS Applied Materials & Interfaces, 2014, 6, 3-8.	8.0	20
261	Ternary blend bulk heterojunction photovoltaic cells with an ambipolar small molecule as the cascade material. RSC Advances, 2014, 4, 1087-1092.	3.6	20
262	Enhanced Biological Functions of Human Mesenchymal Stemâ€Cell Aggregates Incorporating Eâ€Cadherinâ€Modified PLGA Microparticles. Advanced Healthcare Materials, 2016, 5, 1949-1959.	7.6	20
263	Fast Self-Healing and Self-Cleaning Anticorrosion Coating Based on Dynamic Reversible Imine and Multiple Hydrogen Bonds. ACS Applied Polymer Materials, 2022, 4, 4709-4718.	4.4	20
264	Plasma nitridation and microstructure of high-k ZrO2 thin films fabricated by cathodic arc deposition. Journal of Crystal Growth, 2005, 277, 422-427.	1.5	19
265	Induced crystallization of rubrene with diazapentacene as the template. Journal of Materials Chemistry, 2012, 22, 4396.	6.7	19
266	First principle simulations on the effects of oxygen vacancy in HfO2-based RRAM. AIP Advances, 2015, 5, .	1.3	19
267	Co-reduction self-assembly of reduced graphene oxide nanosheets coated Cu2O sub-microspheres core-shell composites as lithium ion battery anode materials. Electrochimica Acta, 2015, 176, 434-441.	5.2	19
268	Facet-Dependent Property of Sequentially Deposited Perovskite Thin Films: Chemical Origin and Self-Annihilation. ACS Applied Materials & amp; Interfaces, 2016, 8, 32366-32375.	8.0	19
269	Direct Observation of Charge Injection of Graphene in the Graphene/WSe <sub>2</sub> Heterostructure by Optical-Pump Terahertz-Probe Spectroscopy. ACS Applied Materials & Interfaces, 2019, 11, 47501-47506.	8.0	19
270	A centrifugal microfluidic pressure regulator scheme for continuous concentration control in droplet-based microreactors. Lab on A Chip, 2019, 19, 3870-3879.	6.0	19

#	Article	IF	CITATIONS
271	The selection strategy of ammonium-group organic salts in vapor deposited perovskites: From dimension regulation to passivation. Nano Energy, 2021, 84, 105893.	16.0	19
272	Identifying conducting phase from the insulating matrix in percolating metal-insulator nanocomposites by conducting atomic force microscopy. Applied Physics A: Materials Science and Processing, 1998, 66, S1171-S1174.	2.3	18
273	Local study of thickness-dependent electronic properties of ultrathin silicon oxide near SiO2/Si interface. Journal Physics D: Applied Physics, 2007, 40, 2886-2893.	2.8	18
274	Photoelectron spectroscopic investigation of nitrogen chemical states in ZnO: (N,Ga) thin films. Journal of Applied Physics, 2008, 103, .	2.5	18
275	Localized Nanodiamond Crystallization and Field Emission Performance Improvement of Amorphous Carbon upon Laser Irradiation in Liquid. Journal of Physical Chemistry C, 2009, 113, 12154-12161.	3.1	18
276	Correlation between Molecular Packing and Surface Potential at Vanadyl Phthalocyanine/HOPG Interface. Journal of Physical Chemistry C, 2010, 114, 19044-19047.	3.1	18
277	hE-cadherin–Fc fusion protein coated surface enhances the adhesion and proliferation of human mesenchymal stem cells. Colloids and Surfaces B: Biointerfaces, 2013, 109, 97-102.	5.0	18
278	Cripto-1 expression in patients with clear cell renal cell carcinoma is associated with poor disease outcome. Journal of Experimental and Clinical Cancer Research, 2019, 38, 378.	8.6	18
279	Cascade Typeâ€II 2D/3D Perovskite Heterojunctions for Enhanced Stability and Photovoltaic Efficiency. Solar Rrl, 2020, 4, 2000282.	5.8	18
280	High mobility and low operating voltage ZnGaO and ZnGaLiO transistors with spin-coated Al <sub>2</sub> O <sub>3</sub> as gate dielectric. Journal Physics D: Applied Physics, 2010, 43, 442001.	2.8	17
281	In situ modification of low-cost Cu electrodes for high-performance low-voltage pentacene thin film transistors (TFTs). Organic Electronics, 2013, 14, 775-781.	2.6	17
282	Hole-dominated Fowler–Nordheim tunneling in 2D heterojunctions for infrared imaging. Science Bulletin, 2021, 66, 139-146.	9.0	17
283	Optimization of Effective Thermal Conductivity of Thermal Interface Materials Based on the Genetic Algorithm-Driven Random Thermal Network Model. ACS Applied Materials & Interfaces, 2021, 13, 45050-45058.	8.0	17
284	Probing local leakage current and ferroelectricity of Pb(Zr0.53, Ti0.47)O3/YBa2Cu3O7â^'x heterostructure by a modified atomic force microscope. Applied Physics Letters, 2000, 76, 1923-1925.	3.3	16
285	Magnetic properties of Fe+-implanted silica films after post-implantation annealing. Journal of Applied Physics, 2000, 88, 2745-2749.	2.5	16
286	Tunneling current and thickness inhomogeneities of ultrathin aluminum oxide films in magnetic tunneling junctions. Journal of Applied Physics, 2001, 90, 5202-5207.	2.5	16
287	Magnetic force microscopy study of domain structures in magnetoresistance (Ni74Fe16Co10)xAg1â^'x granular films. Materials Characterization, 2002, 48, 153-158.	4.4	16
288	Photoelectric effect and transport properties of a single CdS nanoribbon. Ultramicroscopy, 2005, 105, 275-280.	1.9	16

#	Article	IF	CITATIONS
289	Hole size dependence of forward emission from organic dyes coated with two-dimensional metallic arrays. Applied Physics Letters, 2009, 94, 241114.	3.3	16
290	Derivitization of pristine graphene for bulk heterojunction polymeric photovoltaic devices. Journal of Materials Chemistry, 2012, 22, 16723.	6.7	16
291	Variable electronic properties of lateral phosphorene–graphene heterostructures. Physical Chemistry Chemical Physics, 2015, 17, 31685-31692.	2.8	16
292	Size and crystallinity control of dispersed VO <sub>2</sub> particles for modulation of metal–insulator transition temperature and hysteresis. CrystEngComm, 2019, 21, 5749-5756.	2.6	16
293	Spiral growth of GaAs by metalorganic vapor phase epitaxy. Applied Physics Letters, 1994, 64, 1959-1961.	3.3	15
294	Ion implanted nanostructures on Ge(111) surfaces observed by atomic force microscopy. Journal of Vacuum Science & Technology an Official Journal of the American Vacuum Society B, Microelectronics Processing and Phenomena, 1997, 15, 809.	1.6	15
295	Electrical switching behavior from ultrathin potential barrier of self-assembly molecules tuned by interfacial charge trapping. Applied Physics Letters, 2010, 96, .	3.3	15
296	Liquid nitrogen driven assembly of nanomaterials into spongy millispheres for various applications. Journal of Materials Chemistry A, 2018, 6, 5984-5992.	10.3	15
297	Efficient passivation of monolayer MoS2 by epitaxially grown 2D organic crystals. Science Bulletin, 2019, 64, 1700-1706.	9.0	15
298	Tertiary Amines Differentiated from Primary and Secondary Amines by Active Esterâ€Functionalized Hexabenzoperylene in Field Effect Transistors. Chemistry - an Asian Journal, 2019, 14, 1676-1680.	3.3	15
299	Intrinsic memristive mechanisms in 2D layered materials for high-performance memory. Journal of Applied Physics, 2021, 129, .	2.5	15
300	Ultraâ€Narrowband Photodetector with High Responsivity Enabled by Integrating Monolayer Jâ€Aggregate Organic Crystal with Graphene. Advanced Optical Materials, 2021, 9, 2100158.	7.3	15
301	Unveiling the role of filler surface energy in enhancing thermal conductivity and mechanical properties of thermal interface materials. Composites Part A: Applied Science and Manufacturing, 2022, 157, 106904.	7.6	15
302	Spiral growth of GaAs by molecular beam epitaxy. Applied Physics Letters, 1994, 65, 1552-1554.	3.3	14
303	Energetic ion impacts on quartz surfaces: a study by atomic force microscopy. Nuclear Instruments & Methods in Physics Research B, 1996, 118, 473-477.	1.4	14
304	Characterizations of GaN films grown with indium surfactant by RF-plasma assisted molecular beam epitaxy. Microelectronics Reliability, 2002, 42, 1179-1184.	1.7	14
305	Nanoscale investigation on nature of dark hole in moisture-exposed tris(8-hydroxyquinoline) aluminum thin films. Chemical Physics Letters, 2003, 374, 656-660.	2.6	14
306	Preparation and characterization of Ba2TiSi2O8 ferroelectric films produced by sol–gel method. Materials Letters, 2004, 58, 2927-2931.	2.6	14

#	Article	IF	CITATIONS
307	Effect of exciplex formation on organic light emitting diodes based on rare-earth complex. Journal of Applied Physics, 2006, 100, 024506.	2.5	14
308	Optimizing the growth of vanadyl-phthalocyanine thin films for high-mobility organic thin-film transistors. Journal of Applied Physics, 2007, 102, 103711.	2.5	14
309	A low-temperature, solution-processed high- <i>k</i> dielectric for low-voltage, high-performance organic field-effect transistors (OFETs). Journal Physics D: Applied Physics, 2013, 46, 095105.	2.8	14
310	Size Modulation and Heterovalent Doping Facilitated Hybrid Organic and Perovskite Quantum Dot Bulk Heterojunction Solar Cells. ACS Applied Energy Materials, 2020, 3, 11359-11367.	5.1	14
311	Advances in graphene-based polymer composites with high thermal conductivity. Veruscript Functional Nanomaterials, 2018, 2, 1-17.	0.2	14
312	Generation and Detection of Strain-Localized Excitons in WS <sub>2</sub> Monolayer by Plasmonic Metal Nanocrystals. ACS Nano, 2022, 16, 10647-10656.	14.6	14
313	Growth mechanism of GaAs by metalorganic vapor phase epitaxy. Applied Physics Letters, 1994, 64, 2105-2107.	3.3	13
314	Field emission characteristics of SiC capped Si tip array by ion beam synthesis. Journal of Vacuum Science and Technology A: Vacuum, Surfaces and Films, 1999, 17, 2109-2112.	2.1	13
315	Structural, morphological and optical properties of C60cluster thin films produced by thermal evaporation under argon gas. Journal of Physics Condensed Matter, 2001, 13, 2883-2889.	1.8	13
316	Visualization of thermally activated morphology evolution of N, N'-di(naphthalene-1-yl)- N, N'-diphthalbenzidine films on ITO/copper phthalocyanine underlying layer. Applied Physics A: Materials Science and Processing, 2005, 81, 1151-1156.	2.3	13
317	Limit of Voc in polymeric bulk heterojunction solar cells predicted by a double-junction model. Solar Energy Materials and Solar Cells, 2013, 108, 17-21.	6.2	13
318	Artificial Biomimicking Matrix Modifications of Nanofibrous Scaffolds by hE-Cadherin-Fc Fusion Protein to Promote Human Mesenchymal Stem Cells Adhesion and Proliferation. Journal of Nanoscience and Nanotechnology, 2014, 14, 4007-4013.	0.9	13
319	Structure-induced variation of thermal conductivity in epoxy resin fibers. Nanoscale, 2017, 9, 10585-10589.	5.6	13
320	Bulk Heterojunction Quasi-Two-Dimensional Perovskite Solar Cell with 1.18 V High Photovoltage. ACS Applied Materials & Interfaces, 2019, 11, 2935-2943.	8.0	13
321	Numerical homogenization of thermal conductivity of particle-filled thermal interface material by fast Fourier transform method. Nanotechnology, 2021, 32, 265708.	2.6	13
322	Probing electron conduction at the microscopic level in percolating nanocomposites by conducting atomic-force microscopy. Physical Review B, 1998, 57, R15120-R15123.	3.2	12
323	Optical and xerographic properties of phthalocyanine codeposited composite film and ultrathin multilayered structure. Journal of Applied Physics, 2002, 91, 748-752.	2.5	12
324	Nanoscale study on origins of the bright clusters in/on moisture-exposed tris(8-hydroxyquinoline) aluminum thin films. Synthetic Metals, 2004, 145, 177-182.	3.9	12

#	Article	IF	CITATIONS
325	Visualization of thermally-activated degradation pathways of tris(8-hydroxyquinoline) aluminum thin films for electroluminescence application. Thin Solid Films, 2005, 491, 317-322.	1.8	12
326	Low-voltage flexible pentacene thin film transistors with a solution-processed dielectric and modified copper source–drain electrodes. Journal of Materials Chemistry C, 2013, 1, 2585.	5.5	12
327	Enhanced efficiency of organic solar cells by mixed orthogonal solvents. Organic Electronics, 2014, 15, 2007-2013.	2.6	12
328	Controlled Synthesis of MoxW1–xTe2 Atomic Layers with Emergent Quantum States. ACS Nano, 2021, 15, 11526-11534.	14.6	12
329	Synthesis and microstructural properties of tetrahedral amorphous carbon films. Journal of Non-Crystalline Solids, 1999, 254, 161-166.	3.1	11
330	Effects of an oxygen environment on the electrical properties of a single CdS nanobelt device. Nanotechnology, 2011, 22, 135702.	2.6	11
331	Carrier sheet density constrained anomalous current saturation of graphene field effect transistors: kinks and negative differential resistances. Nanoscale, 2013, 5, 2811.	5.6	11
332	Observation of viscoelasticity in boron nitride nanosheet aerogel. Physical Chemistry Chemical Physics, 2015, 17, 16709-16714.	2.8	11
333	A self-driven approach for local ion intercalation in vdW crystals. Nanoscale, 2020, 12, 1448-1454.	5.6	11
334	Bifunctional Effects of Trichloro(octyl)silane Modification on the Performance and Stability of a Perovskite Solar Cell via Microscopic Characterization Techniques. ACS Applied Energy Materials, 2020, 3, 3302-3309.	5.1	11
335	Aggregation and out diffusion of iron atoms for Fe ion implanted silica films. Journal of Applied Physics, 1999, 86, 2550-2554.	2.5	10
336	Construction and characterization of a heating stage for a scanning probe microscope up to 215 °C. Review of Scientific Instruments, 2000, 71, 2100-2103.	1.3	10
337	Studying the high-field electron conduction of tetrahedral amorphous carbon thin films by conducting atomic force microscopy. Materials Characterization, 2002, 48, 205-210.	4.4	10
338	Effects of sputtering pressure on compositions and structures of fresnoite thin films. Physica B: Condensed Matter, 2005, 355, 100-105.	2.7	10
339	Unusual electronic and magnetic properties of lateral phosphorene–WSe2 heterostructures. Journal of Materials Chemistry C, 2016, 4, 6657-6665.	5.5	10
340	Structural Regulation for Highly Efficient and Stable Perovskite Solar Cells via Mixed-Vapor Deposition. ACS Applied Energy Materials, 2020, 3, 6544-6551.	5.1	10
341	A spontaneously formed plasmonic-MoTe2 hybrid platform for ultrasensitive Raman enhancement. Cell Reports Physical Science, 2021, 2, 100526.	5.6	10
342	Spiral growth of InP by metalorganic vapor phase epitaxy. Applied Physics Letters, 1994, 65, 1394-1396.	3.3	9

#	Article	IF	CITATIONS
343	Step flow growth of (La,Ca)MnOδ thin films on (110)NdGaO3. Applied Physics Letters, 1995, 67, 3272-3274.	3.3	9
344	Domain Structure Investigations of Triglycine Sulfo-Phosphate Single Crystal: Evidence of Domain Motion with Time at Room Temperature. Japanese Journal of Applied Physics, 1997, 36, 4377-4381.	1.5	9
345	Ferroelectric relaxation of (Pb0.76Ca0.24)TiO3 thin film. Solid State Communications, 2002, 121, 603-607.	1.9	9
346	Influence of surface morphology on the field emission properties of planar SiC/Si heterostructures formed by ion beam synthesis. Solid State Communications, 2003, 128, 435-439.	1.9	9
347	Electron Beam Induced Light Emission and Charge Conduction Patterning in ZnO by Using an AlOx Layer. Advanced Materials, 2005, 17, 1960-1964.	21.0	9
348	Co doped ZnO(0001)-Zn by diffusion method and its magnetic properties. Applied Physics Letters, 2009, 95, .	3.3	9
349	Improving the Quality of the Si/Cu <sub>2</sub> O Interface by Methylâ€Group Passivation and Its Application in Photovoltaic Devices. Advanced Materials Interfaces, 2017, 4, 1600833.	3.7	9
350	Defect Etching of Phaseâ€Transitionâ€Assisted CVDâ€Grown 2Hâ€MoTe <sub>2</sub> . Small, 2021, 17, e2102	1460.0	9
351	Phase-controlled epitaxial growth of MoTe2: Approaching high-quality 2D materials for electronic devices with low contact resistance. Journal of Applied Physics, 2022, 131, .	2.5	9
352	Abnormally high thermal conductivity in fivefold twinned diamond nanowires. Materials Today Physics, 2022, 25, 100705.	6.0	9
353	Proposal to study the thermopower produced by a vacuum-tunneling junction. Journal of Vacuum Science & Technology an Official Journal of the American Vacuum Society B, Microelectronics Processing and Phenomena, 1994, 12, 2156.	1.6	8
354	Epitaxial regrowth of Ge films on (001) GaAs byin situthermal pulse annealing of evaporated amorphous germanium. Applied Physics Letters, 1997, 70, 865-867.	3.3	8
355	Tip artifacts in atomic force microscope imaging of ion bombarded nanostructures on germanium surfaces. Journal of Applied Physics, 1997, 82, 5859-5861.	2.5	8
356	Low-temperature preparation of self-polarized Pb(Mg1/3Nb2/3)O3–PbTiO3 films on well crystallized LaNiO3 electrodes. Journal of Alloys and Compounds, 2013, 577, 606-609.	5.5	8
357	Configuration-dependent electronic and magnetic properties of graphene monolayers and nanoribbons functionalized with aryl groups. Journal of Chemical Physics, 2014, 140, 044712.	3.0	8
358	Enhanced Photoresponse in Interfacial Gated Graphene Phototransistor With Ultrathin Al <sub>2</sub> O <sub>3</sub> Dielectric. IEEE Electron Device Letters, 2018, 39, 987-990.	3.9	8
359	Observation of Strong <i>J</i> -Aggregate Light Emission in Monolayer Molecular Crystal on Hexagonal Boron Nitride. Journal of Physical Chemistry A, 2020, 124, 7340-7345.	2.5	8
360	Enhanced thermo-optic nonlinearities in a MoS <sub>2</sub> -on-silicon microring resonator. Applied Physics Express, 2020, 13, 022004.	2.4	8

#	Article	IF	CITATIONS
361	Growth dynamics and photoresponse of the Wadsley phase V <sub>6</sub> O <sub>13</sub> crystals. Journal of Materials Chemistry C, 2020, 8, 6470-6477.	5.5	8
362	Characterization and giant magnetoresistance effect in cobalt–silver granular films formed by MEVVA implantation. Nuclear Instruments & Methods in Physics Research B, 1999, 148, 813-818.	1.4	7
363	Variable-Temperature Scanning Tunneling Microscopy and Scanning Tunneling Spectroscopy Study on Copper Phthalocyanine Ultrathin Films on a Au(111) Surface. Journal of Nanoscience and Nanotechnology, 2002, 2, 139-142.	0.9	7
364	Tip Effects of Piezoelectric-Mode Atomic Force Microscope for Local Piezoelectric Measurements of an SrBi2Ta2O9Thin Film. Japanese Journal of Applied Physics, 2002, 41, 6793-6796.	1.5	7
365	Ferroelectric domain configuration and piezoelectric responses in (001)-oriented PMN-PT films. Materials Characterization, 2002, 48, 215-220.	4.4	7
366	Studies of the effects of ion irradiation on ferroelectric domains of triglycine sulfate single crystals on a nanometer scale. Physics Letters, Section A: General, Atomic and Solid State Physics, 2003, 309, 121-125.	2.1	7
367	Fabrication of rutile TiO2 thin films by low-temperature, bias-assisted cathodic arc deposition and their dielectric properties. Journal of Materials Research, 2006, 21, 844-850.	2.6	7
368	Influence of Annealing on Raman Spectrum of Graphene in Different Gaseous Environments. Spectroscopy Letters, 2014, 47, 465-470.	1.0	7
369	A novel solid-to-solid electrocatalysis of graphene oxide reduction on copper electrode. RSC Advances, 2015, 5, 87987-87992.	3.6	7
370	Surface morphology of nitrogen doped tetrahedral amorphous carbon films on silicon by atomic microscopy imaging. Materials Letters, 1998, 34, 1-4.	2.6	6
371	Alternate heteroepitaxial growth of chloroindium phthalocyanine and chloroaluminum phthalocyanine ultrathin multilayered structure and its xerographic and optical properties. Thin Solid Films, 2001, 384, 109-114.	1.8	6
372	Electron field emission characteristics of textured silicon surface. Journal of Vacuum Science & Technology an Official Journal of the American Vacuum Society B, Microelectronics Processing and Phenomena, 2001, 19, 884.	1.6	6
373	Stable field emission with low threshold field from amorphous carbon films due to layer-by-layer hydrogen plasma annealing. Journal of Applied Physics, 2002, 91, 5434-5437.	2.5	6
374	A model for exciton formation in organic electroluminescent devices. Solid-State Electronics, 2002, 46, 645-650.	1.4	6
375	Microstructure control of sputtered Ba2TiSi2O8 films by sol–gel-derived underlayer. Journal of Crystal Growth, 2005, 285, 117-122.	1.5	6
376	Dependence of anisotropic surface plasmon lifetimes of two-dimensional hole arrays on hole geometry. Applied Physics Letters, 2009, 95, 063110.	3.3	6
377	Quantum confinement and electron spin resonance characteristics in Si-implanted silicon oxide films. Journal of Applied Physics, 2011, 109, 084502.	2.5	6
378	TFSA doped interlayer for efficient organic solar cells. Organic Electronics, 2014, 15, 3702-3709.	2.6	6

#	Article	IF	CITATIONS
379	Rapid growth of high quality perovskite crystal by solvent mixing. CrystEngComm, 2016, 18, 1184-1189.	2.6	6
380	Experimental Observation of Ultrahigh Mobility Anisotropy of Organic Semiconductors in the Two-Dimensional Limit. ACS Applied Electronic Materials, 2020, 2, 2888-2894.	4.3	6
381	Towards Scalable Fabrications and Applications of 2D Layered Material-based Vertical and Lateral Heterostructures. Chemical Research in Chinese Universities, 2020, 36, 525-550.	2.6	6
382	Towards low-voltage organic thin film transistors (OTFTs) with solution-processed high- <em>k</em> dielectric and interface engineering. AIMS Materials Science, 2015, 2, 510-529.	1.4	6
383	Investigation on the Fano-Type Asymmetry in Atomic Semiconductor Coupled to the Plasmonic Lattice. ACS Photonics, 2021, 8, 3583-3590.	6.6	6
384	Dendritic crystallization of amorphous germanium byin situthermal pulse annealing. Journal of Applied Physics, 1997, 81, 7757-7763.	2.5	5
385	Atomic force microscopy study of microcrystalline SiC fabricated by ion beam synthesis. Journal of Vacuum Science and Technology A: Vacuum, Surfaces and Films, 1998, 16, 968-973.	2.1	5
386	Ion beam synthesized cobalt germanide alloy by metal vapor vacuum arc implantation. Nuclear Instruments & Methods in Physics Research B, 1999, 148, 604-609.	1.4	5
387	Conductance distribution in granular metal films: a combined study by conducting atomic force microscopy and computer simulation. Physica B: Condensed Matter, 2000, 279, 98-101.	2.7	5
388	Compositional and morphological study of reactive ion beam deposited AlN thin films. Nuclear Instruments & Methods in Physics Research B, 2000, 169, 94-97.	1.4	5
389	Magnetic domain structures and giant magnetoresistance of granular (Ni[sub 74]Fe[sub 16]Co[sub) Tj ETQq1 1	0.784314	4 rgBT /Oved
390	Ion channeling studies on mixed phases formed in metalorganic chemical vapor deposition grown Mg-doped GaN on Al2O3(0001). Journal of Applied Physics, 2000, 87, 955-957.	2.5	5
391	Dispersion, refinement, and manipulation of single silicon nanowires. Applied Physics Letters, 2002, 80, 1812-1814.	3.3	5
392	Preparation of (100)-Oriented LaNiO3Oxide Electrodes for SrBi2Ta2O9-Based Ferroelectric Capacitors. Japanese Journal of Applied Physics, 2002, 41, 6877-6881.	1.5	5
393	In situfabrication and characterization of tungsten nanodots on SiO2/Si via field induced nanocontact with a scanning tunnelling microscope. Nanotechnology, 2005, 16, 2993-3000.	2.6	5
394	Facile modification of Cu source–drain (S/D) electrodes for high-performance, low-voltage n-channel organic thin film transistors (OTFTs) based on C 60. Organic Electronics, 2014, 15, 3259-3267.	2.6	5
395	A Study on the Factors about Customers' Acceptability to Airline Ancillary Products. Procedia Computer Science, 2017, 107, 39-46.	2.0	5
396	Serum chitinase activity prognosticates metastasis of colorectal cancer. BMC Cancer, 2019, 19, 629.	2.6	5

#	Article	IF	CITATIONS
397	The Impact of PbI 2 :KI Alloys on the Performance of Sequentially Deposited Perovskite Solar Cells. European Journal of Inorganic Chemistry, 2021, 2021, 821-830.	2.0	5
398	Effect of defect on the programming speed of charge trapping memories. Wuli Xuebao/Acta Physica Sinica, 2014, 63, 053101.	0.5	5
399	Effect of hydrogen bonds on the thermal transport in a precisely branched polyethylene with ordered and amorphous structures. Computational Materials Science, 2022, 205, 111191.	3.0	5
400	Spiral growth of GaAs by metalorganic vapor phase epitaxy. Journal of Vacuum Science & Technology an Official Journal of the American Vacuum Society B, Microelectronics Processing and Phenomena, 1994, 12, 2115.	1.6	4
401	Crystallization of ion-beam-synthesized SiC layer by thermal annealing. Applied Physics A: Materials Science and Processing, 1998, 66, S539-S543.	2.3	4
402	Optical properties in infra-red region of nitrogen-incorporated amorphous carbon films. Diamond and Related Materials, 1998, 7, 491-494.	3.9	4
403	Electroluminescence from ZnSTe:Al alloy and investigation of local current distributions by conducting atomic force microscopy. Journal of Vacuum Science & Technology an Official Journal of the American Vacuum Society B, Microelectronics Processing and Phenomena, 1998, 16, 14.	1.6	4
404	Probing conducting particles buried in a Ni[sub x](SiO[sub 2])[sub 1â^'x] composite by conducting atomic force microscopy. Journal of Vacuum Science & Technology an Official Journal of the American Vacuum Society B, Microelectronics Processing and Phenomena, 1998, 16, 1953.	1.6	4
405	Atomic Force Microscope Studies on Domain Dynamics in Phosphate Substituted Triglycine Sulfate Single Crystals: Evidence for the Domain Boundary Motion towards Negative Region and Holes Formation at the Domain Boundary. Japanese Journal of Applied Physics, 1998, 37, 6177-6182.	1.5	4
406	Studies of leakage current inhomogeneity of Pb(Zr, Ti)O3/YBa2Cu3Ox heterostructures on a nanometer scale. Journal of Non-Crystalline Solids, 1999, 254, 112-117.	3.1	4
407	Study of polarization switching in PZT films with RuO2 electrodes by conducting atomic force microscopy. Materials Characterization, 2002, 48, 249-253.	4.4	4
408	Plasma-nitrided high-k polycrystalline nano-array induced by electron irradiation. Nanotechnology, 2006, 17, 4379-4383.	2.6	4
409	Electron interferometry in the proximity of amorphous ultrathin SiO2â^•Si. Applied Physics Letters, 2007, 90, 182108.	3.3	4
410	In situ characterization of initial growth of HfO2. Applied Physics Letters, 2009, 94, 032904.	3.3	4
411	Super-linear rectifying property of rubrene single crystal devices. Organic Electronics, 2011, 12, 1731-1735.	2.6	4
412	Annealing effect on relaxor behaviours of spark plasma sintered Pb(Sc <sub>1/2</sub> Nb <sub>1/2</sub> )O <sub>3</sub> superfine ceramics. Advances in Applied Ceramics, 2011, 110, 74-79.	1.1	4
413	Low-voltage graphene field-effect transistors based on octadecylphosphonic acid modified solution-processed high- <i>k</i> dielectrics. Nanotechnology, 2014, 25, 265201.	2.6	4
414	Design of a novel double doping polysilicon gate MOSFET. Materials Science in Semiconductor Processing, 2015, 31, 229-234.	4.0	4

#	Article	IF	CITATIONS
415	Thermal and illumination effects on a Pbl <sub>2</sub> nanoplate and its transformation to CH <sub>3</sub> NH <sub>3</sub> Pbl <sub>3</sub> perovskite. CrystEngComm, 2019, 21, 736-740.	2.6	4
416	LYPD8 regulates the proliferation and migration of colorectal cancer cells through inhibiting the secretion of ILâ€'6 and TNFâ€'α. Oncology Reports, 2019, 41, 2389-2395.	2.6	4
417	Ordered orientation of silicon carbide nanowires in polymer composites for enhanced permittivity and energy storage density. Materials Chemistry and Physics, 2020, 249, 122993.	4.0	4
418	A Novel Organic Substrate with Enhanced Thermal Conductivity. , 2017, , .		4
419	40 GHz waveguide-integrated two-dimensional palladium diselenide photodetectors. Applied Physics Letters, 2022, 120, .	3.3	4
420	Characterization of nano-sized Si islands in buried oxide layer of SIMOX by conducting AFM. Chemical Physics Letters, 2003, 376, 748-752.	2.6	3
421	XTEM characterization of tungsten implanted SiC thin films on silicon for field emission devices. Thin Solid Films, 2003, 427, 417-421.	1.8	3
422	Nanoscale structural characteristics and electron field emission properties of transition metal–fullerene compound TiC60 films. Microelectronics Reliability, 2005, 45, 137-142.	1.7	3
423	Self-assembly of carbon nanoclusters on dielectric boron nitride. Applied Surface Science, 2014, 292, 237-246.	6.1	3
424	A 2-D semi-analytical model of double-gate tunnel field-effect transistor. Journal of Semiconductors, 2015, 36, 054002.	3.7	3
425	Grain boundary enhanced oxygen out-diffusion in annealed polycrystalline Si/SiO2/crystalline Si structures. Thin Solid Films, 1996, 286, 317-320.	1.8	2
426	Morphology and characteristics of C60 thin films grown in argon atmosphere by thermal evaporation. Journal of Vacuum Science and Technology A: Vacuum, Surfaces and Films, 2001, 19, 1018-1021.	2.1	2
427	Sample refinement and manipulation of silicon nanowires. Materials Characterization, 2002, 48, 177-181.	4.4	2
428	Self-assembled growth of nanostructural Ge islands on bromine-passivated Si(111) surfaces at room temperature. Pramana - Journal of Physics, 2002, 59, 133-142.	1.8	2
429	Ellipsometric Spectra and Optical Properties of Anisotropic SrBi 2 Ta 2 O 9 Films. Chinese Physics Letters, 2004, 21, 266-268.	3.3	2
430	Synthesis of Multishell Carbon Nanotube Composites via Template Method. Chinese Journal of Chemical Physics, 2011, 24, 206-210.	1.3	2
431	Study of the electron standing wave states in scanning tunneling spectroscopy of Si(111) surface. Surface and Interface Analysis, 2013, 45, 962-967.	1.8	2
432	Self-assembled dipoles of <i>o</i> -carborane on gate oxide tuning charge carriers in organic field effect transistors. Journal of Materials Chemistry C, 2022, 10, 2690-2695.	5.5	2

#	Article	IF	CITATIONS
433	Graphene nano-optomechanical resonators on an integrated photonic platform. , 2018, , .		2
434	"Resonant conducting―in nano-patterning the hydrogen-passivated Si(100) by atomic force microscopy. Applied Physics Letters, 1997, 71, 2035-2037.	3.3	1
435	Single ion impacts on an In0.22Ga0.78As/GaAs(100) surface observed by atomic force microscopy. Nuclear Instruments & Methods in Physics Research B, 1997, 124, 500-505.	1.4	1
436	Morphology of MBE grown InAs films studied by atomic force microscope. Journal of Crystal Growth, 1997, 175-176, 1289-1293.	1.5	1
437	Aging effect on the ferroelectric property of YMnO3thin film. Ferroelectrics, 2001, 259, 181-185.	0.6	1
438	Synthesis and characterization of SrTiO/sub 3/ thin films by a modified metalorganic decomposition technique. , 0, , .		1
439	Title is missing!. Journal of Materials Science: Materials in Electronics, 2002, 13, 419-424.	2.2	1
440	Novel molecular device based on electrostatic interactions in organic polymers. , 0, , .		1
441	Temperature dependence of surface plasmon mediated near band-edge emission from Ag/ZnO nanorods. Journal of Optics (United Kingdom), 2011, 13, 075003.	2.2	1
442	Reversible Ferromagnetism Study in Un-Doped ZnO Thin Films. Journal of Nanoscience and Nanotechnology, 2011, 11, 10557-10561.	0.9	1
443	Manipulation of Graphene Properties by Interface Engineering. ECS Transactions, 2011, 37, 133-139.	0.5	1
444	Intermolecular Coupling Related Electrical Transport Transition in Vanadyl-Phthalocyanine (VOPc) Molecular Bilayers. Journal of Physical Chemistry C, 2012, 116, 17580-17585.	3.1	1
445	Polarization dependent loss of graphene-on-silicon waveguides. , 2013, , .		1
446	Dressing plasmon resonance with particle-microcavity architecture for efficient nano-optical trapping and sensing. Optics Letters, 2014, 39, 873.	3.3	1
447	Thermal property analysis of boron nitride-filled glass-fiber reinforced polymer composites. , 2014, , .		1
448	Effect of functionalized multiwalled carbon nanotubes on the coefficient of thermal expansion of bismaleimide-triazine resins (BT resins). , 2015, , .		1
449	Two-dimensional semi-analytical model of subthreshold surface potential and drain current for double-doping polysilicon gate MOSFET. Japanese Journal of Applied Physics, 2015, 54, 054202.	1.5	1
450	Novel continuously-tunable memristor based on few-layers black		1

phosphorus/MoS<inf&gt;2&lt;/inf&gt; heterojunction. , 2016, , .

#	Article	IF	CITATIONS
451	Effect of silver nanoparticles decoration on the thermal conductivity of boron nitride nanosheets/silicon carbide nanowires bioinspired composite paper. , 2016, , .		1
452	Thermal Conductivity: Manipulating Orientation of Silicon Carbide Nanowire in Polymer Composites to Achieve High Thermal Conductivity (Adv. Mater. Interfaces 17/2017). Advanced Materials Interfaces, 2017, 4, .	3.7	1
453	Terahertz Microfluidic Metamaterial Biosensor for Tiny Volume Liquid Samples. , 2018, , .		1
454	Facile Preparation of Silver Nanoparticles Decorated Boron Nitride Nanotube Hybrids. , 2018, , .		1
455	Aligned-carbon-fibre/Silicone-rubber Composite with High Thermal Conductivity Fabricated by Double-stacked Electrostatic Flocking Method. , 2020, , .		1
456	Facile Fabrication of Silicon Carbide Spheres and Its Application in Polymer Composites with Enhanced Thermal Conductivity. , 2020, , .		1
457	Topology Optimization Design Of Meta-Material Heat Spreader. , 2021, , .		1
458	Graphene-assisted electro-optomechanical integration on a silicon-on-insulator platform. Optics Express, 2020, 28, 14386.	3.4	1
459	Surface morphology of metalorganic vapor phase epitaxy grown InAs and InGaAs observed by atomic force microscopy. Journal of Vacuum Science & Technology an Official Journal of the American Vacuum Society B, Microelectronics Processing and Phenomena, 1996, 14, 1105.	1.6	0
460	A study of ion-bombarded nanostructures on germanium surfaces by scanning probe microscopy. Thin Solid Films, 1997, 308-309, 415-419.	1.8	0
461	An STM and atomic force microscopy study of the effects of 1.8 MeV electron bombardment on the surface of graphite. Journal of Materials Science, 1998, 33, 4657-4663.	3.7	Ο
462	Room temperature visible photoluminescence from crystallized nano-Si thin films. Journal of Non-Crystalline Solids, 1998, 227-230, 1045-1048.	3.1	0
463	Surface roughness and oxide contents of gas-phase and solution-phase polysulfide passivation of III–V surfaces. Journal of Vacuum Science and Technology A: Vacuum, Surfaces and Films, 1999, 17, 93-96.	2.1	Ο
464	Magnetoresistance properties of ion beam synthesized granular magnetic thin films. Nuclear Instruments & Methods in Physics Research B, 2000, 169, 166-173.	1.4	0
465	VERY LOW THRESHOLD ELECTRON FIELD EMISSION FROM AMORPHOUS CARBON FILMS WITH HYDROGEN DILUTION. International Journal of Modern Physics B, 2002, 16, 988-992.	2.0	Ο
466	Resonant Rutherford backscattering spectrometry and channeling studies on the effect of annealing of La0.67Ca0.33MnO3 epilayers grown on SrTiO3() substrates using a facing-target sputtering technique. Nuclear Instruments & Methods in Physics Research B, 2002, 188, 84-89.	1.4	0
467	Scaling analysis of Fe-implanted Ge surfaces using atomic force microscopy. Materials Characterization, 2002, 48, 241-247.	4.4	0
468	Electrons resonant tunnelling between a metal tip and ultrathin silicon oxide on Si(111). , 0, , .		0

#	Article	IF	CITATIONS
469	Micro-structural characteristics and electron field emission properties of transition metal-fullerene compound TiC/sub 60/ films. , 0, , .		0
470	Local Study of DC and Dynamic Electrical Stress Induced Ultrathin Gate Oxide Soft-Breakdown by Scanning Tunneling Microscopy. , 0, , .		0
471	Light emission and charge transport studies on ZnO heterostructures. , 2006, , .		0
472	Reversible ferromagnetism study in un-doped ZnO thin film. , 2010, , .		0
473	Probing the thermal decomposition behaviors of ultrathin HfO <sub>2</sub> films by an <i>in situ</i> high temperature scanning tunneling microscope. Nanotechnology, 2011, 22, 195705.	2.6	0
474	Stability Improvement of Polymer Based Solar Cells by Thermally Evaporated Cr2O3 Interfacial Layer. Materials Research Society Symposia Proceedings, 2011, 1312, 1.	0.1	0
475	P-N Junction Formation in Electron-beam Irradiated Graphene Step. Materials Research Society Symposia Proceedings, 2012, 1407, 224.	0.1	0
476	Preparation and characterization of carbon nanotube@SiO <inf>2</inf> core-shell nanoparticles. , 2013, , .		0
477	Characterization of Metallo-porphine Monolayer and Bilayer on Ag(111): Screening of Substrate Effects. Applied Mechanics and Materials, 2014, 618, 225-232.	0.2	0
478	Study on the bridge effect of graphene oxide on thermal conductivity of Al <inf>2</inf> O <inf>3</inf> filled glass fibers reinforced polymer composites. , 2014, , .		0
479	Curing mechanism and thermal properties of a certain liquid crystalline epoxy resin cured with different curing agents. , 2014, , .		0
480	A testing system for thermal properties of solar gravity heat-pipes. , 2015, , .		0
481	Nonlinear adaptive power capture control of variable-speed wind energy conversion systems using online approximators. , 2015, , .		0
482	Facile synthesis of silver nanoparticles decorated boron nitride nanosheets hybrids. , 2015, , .		0
483	Broadband terahertz modulation using SiO <inf>2</inf> /Si gated monolayer graphene. , 2016, , .		0
484	Designed Stem Cell Aggregates: Enhanced Biological Functions of Human Mesenchymal Stemâ€Cell Aggregates Incorporating Eâ€Cadherinâ€Modified PLGA Microparticles (Adv. Healthcare Mater. 15/2016). Advanced Healthcare Materials, 2016, 5, 1992-1992.	7.6	0
485	Enhanced thermal conductivity and mechanical properties of epoxy resin-alumina-silicon carbide fibers three-phase composites. , 2016, , .		0
486	Fabrication and thermal conduction mechanism of epoxy/modified SiCNP polymer composites. , 2017, , .		0

#	Article	lF	CITATIONS
487	Effective synthesis of Al <inf>2</inf> O <inf>3</inf> -silver nanoparticles hybrids. , 2017, , .		0
488	Hierarchically interconnected epoxy/BN-SCMC polymer composites with enhanced thermal conductivity. , 2017, , .		0
489	Flexible vertical field-effect transistor based on graphene/silicon heterostructure with ion-gel gate. , 2017, , .		0
490	Silver nanoparticle deposited boron nitride nanosheet/nanofibrillated cellulose composites with enhanced thermal conductivity. , 2017, , .		0
491	A novel graphene oxide millispheres / epoxy resin composite with improved thermal conductivity. , 2018, , .		0
492	Hybrid Integration of Black Phosphorus-WSe <inf>2</inf> Heterojunction Photodetector on Silicon Waveguide. , 2018, , .		0
493	Preparation and Characterization of Al <inf>2</inf> O <inf>3</inf> -AgNP hybrids for Application in Thermally Conductive Polymer Composites. , 2018, , .		0
494	Flexible Graphene-Glass Fiber Composite Film with Ultrahigh Thermal Conductivity and Mechanical Strength as Highly Efficient Thermal Spreader Materials. , 2019, , .		0
495	Narrowband Photodetector by Integrating PTCDI-C13 J-aggregates with Graphene. , 2021, , .		0
496	Numerical analysis of the microscopic factors influencing the thermal conductivity of Al2O3/ AIN polymer composites. , 2021, , .		0
497	Evaluation of Aging Performance of Thermal Gel Subjected to Laser Flash Tests. , 2021, , .		0
498	Preparation and Characterization of Two-Dimensional Layered Transition Metal Dichalcogenide Thin Films. , 2019, , .		0
499	Numerical analysis on the effect of microstructures on the thermal and mechanical properties of carbon fiber / Al2O3 thermal pad. , 2021, , .		0
500	Hybrid two-dimensional-material photonics with bound states in the continuum. , 2020, , .		0
501	Graphene-silicon nitride photodetector with bound state in the continuum. , 2020, , .		0
502	Strong correlation between electrical and thermal transport properties in graphene/graphite films beyond the Wiedemann-Franz law. Carbon, 2022, , .	10.3	0
503	Study on the bridge effect of graphene oxide on thermal conductivity of Al <inf>2</inf> O <inf>3</inf> filled glass fibers reinforced polymer composites. , 2014, , .		0
504	Curing mechanism and thermal properties of a certain liquid crystalline epoxy resin cured with different curing agents. , 2014, , .		0